Bachelorarbeit/Bachelor's Thesis

Computational Dynamics Investigation Of Polymer Topology

verfasst von / submitted by

Eray Koca

angestrebter akademischer Grad / in partial fulfilment of the requirements for the degree of

Bachelor of Science (BSc)

Wien, 2025

Studienkennzahl / degree programme code:	UA 033 676
Fachrichtung / degree programme:	Bachelorstudium Physik
Betreut von / Supervisor:	Univ. -Prof. Dipl. -Ing Dr. Christos Likos

Abstract

This thesis focuses on computational polymer topology investigation. The study initially started with exploring the behavior of linear polymers through simulations, progressing to ring polymers and finally concentrating on double-ring polymers. The primary goal is to gather data via computational simulations and analyse the probability distribution of the geometrical behavior and further geometrical quantities of double-ring polymers.

To advance understanding of polymer topology, this study aims to offer valuable computational insights, that encourage further experimental investigations to validate and build upon theoretical findings, ultimately enhancing the broader understanding of polymers. This work also intends to demonstrate how effectively computational simulations that have been used can investigate statistical properties.

Computational polymer topology analyses investigates polymer structure and properties at the molecular level using various methods and potentials. One crucial method, that is used in this work, is Monte Carlo simulation, which employs random sampling to explore potential polymer configurations. The Metropolis criterion, also known as the Boltzmann acceptance criterion, determines whether proposed movements of the polymer are accepted based on the energy change, following the Boltzmann distribution.

Specific potentials model interactions within polymer structures. The FENE potential (Finitely Extensible Nonlinear Elastic) describes elastic stretching of polymer bonds and prevents unphysical elongations by applying a strong restoring force beyond a certain length limit. The WCA potential (Weeks-Chandler-Andersen), a truncated Lennard-Jones potential, describes short-range repulsive interactions and ensures non-overlapping monomers within a polymer chain, resulting in self-avoiding polymers.

The study defines two vectors originating from the midpoint between the rings to their centers of mass. By applying the Boltzmann distribution and statistically screening double-ring movements, the stiffness of the double ring is analysed. In addition, the gyration-tensor of the polymers, their eigenvalues and gyration-radii can be calculated, and for further understanding analysed.

Overall, despite some deviations in the datasets, the double ring model consistently displays measurable bending rigidity.

Contents

1 Introduction

Understanding polymer topology is crucial for designing materials with tailored properties, as different structures influence mechanical strength, elasticity, thermal behavior, and chemical resistance. Beyond material science, polymer topology plays a key role in biological systems, such as the structural organization of DNA.

Over the years, significant advancements have deepened our understanding of polymer topology. Early developments, including Staudinger's macromolecular theory and Flory and Huggins' statistical models, laid the foundation for studying polymer structures. Later, De Gennes introduced reptation theory to describe polymer dynamics, while knot theory provided a framework for analysing loops and entanglements. More recently, advances in supramolecular chemistry and controlled polymer synthesis have enabled precise topological control, with applications in nanotechnology and biomaterials. [4, 3]

Among various polymer architectures, ring polymers have drawn significant interest due to their unique topological constraints, which affect their physical behavior. Unlike linear polymers, ring polymers lack free ends, leading to distinct dynamic and mechanical properties. However, more complex topologies, such as "self-avoiding double-ring polymers", remain relatively unexplored, despite their potential for material and biological applications.

Recent research of Michiletti et al. [2] explores the behavior of supercoiled ring polymers under shear flow, offering insights into their complex conformational dynamics. Their study combines simulations and theoretical modelling to examine how shear forces influence polymer deformation, relaxation, and entanglement. They demonstrate that supercoiling significantly alters a polymer's response to flow, leading to distinct stretching and tumbling regimes. These findings contribute to understanding the rheology of topologically constrained polymers and provide a framework for investigating more intricate architectures.[6] Their paper also sparked the interest for this work.

This thesis aims to conduct computational simulations to analyse the topological behavior of double-ring polymers. With simulations it examines a geometrical probability distribution and energy development and provide information on the topological characteristics. By doing so, this research advances the understanding of polymer topology and its implications.

1.1 Polymers

To define a polymer, the first step is to identify a monomer, the fundamental building block. Monomers link together over covalent bonds to form polymer chains. One key characteristic used to describe a polymer is the degree of polymerization N, which represents the number of monomers in a polymer chain. This value is expressed as $N = \frac{M}{M_{mon}}$, where M is the number-average molar mass of the polymer, and M_{mon} is the molecular weight of a single monomer. Since polymerization is a statistical process, the degree of polymerization is typically given as an average.

Each polymer consists of a primary chain, known as the backbone, which provides the fundamental structure of the polymer. This micro-structure, the backbone, remains unchanged unless covalent bonds are broken. The length of the backbone, typically measured by the number of monomers it contains, is a key factor in describing the polymer chain.

Furthermore, to determine the mass M of a single molecule, the following relation can be used:

$$M = \frac{M_{mol}}{N_A},$$

where M_{mol} is the molar mass of the molecule, and N_A is Avogadro's number $6.02 \cdot 10^{23} mol^{-1}$.

Additionally to be defined, isomers are molecules that share the same molecular formula but differ in the arrangement or position of their atoms. Isomers can be classified into structural isomers, that are molecules that have different connectivity between atoms and stereo-isomers, that are molecules that have the same connectivity but different spatial orientations.

There are several types of monomers. Ethene or propen are typical example in case of plastics. If the polymer contains only one type of monomer, it is called homopolymers. Polymers that contain monomers of different type are called heteropolymers. DNA is a good example for this case.

Beyond these basic classifications, polymers can also be distinguished by their molecular structure. A polymer can be linear, consisting of long, unbranched chains, or it can be branched, where side chains influence properties such as density and mechanical strength. Some polymers exhibit cross-linking, in which covalent bonds connect different chains, making them more rigid. In cases of extensive cross-linking, polymers form a network structure. Another important distinction is based on their thermal properties. Thermoplastics soften when heated and can be reshaped multiple times, while thermosets undergo an irreversible curing process, meaning they do not melt upon reheating.

The behavior of a polymer is also influenced by intermolecular forces. Van der Waals forces play a role in determining flexibility and packing, while hydrogen bonding strengthens polymer networks, as seen in materials like nylon. In polymers containing polar functional groups, dipole-dipole interactions further impact their structural properties. These structural and molecular properties

influence polymer behavior, setting the stage for understanding ideal versus real polymer chains.

Since polymerization is a statistical process, real polymers consist of chains of varying lengths. This leads to differences in molecular weight, which can be described using different measures. The number-average molecular weight considers all molecules equally, while the weight-average molecular weight gives greater emphasis to larger molecules. The ratio of these two values, known as the polydispersity index (PDI), describes the molecular weight distribution in a polymer sample.

The conformational statistics of polymer chains can be characterized by studying the probability distribution of their end-to-end vector. For a polymer composed of N monomers, the end-to-end vector $\vec{R}$ represents the displacement between the first and last monomer.

1.2 Modelling

1.2.1 Ideal Polymers

In this model, which is the easiest possible, monomers do not interact with each other even when they approach each other in space. That means that a position can be shared by two monomers along the chain. Despite the simplicity of the model, many molecular chains can effectively be modelled as ideal polymers under a specific temperature denoted by θ.

In polymer physics, particularly when dealing with ideal chains, one of the fundamental descriptors of chain dimensions is the mean-squared end-to-end distance, denoted as $\langle R^2 \rangle$. For an ideal chain, this quantity can be expressed as

$$\langle R^2 \rangle = C_n \cdot n \cdot l^2,$$

where n is the total number of segments in the polymer chain, l is the length of each segment, and C_n is a dimensionless constant that reflects the chain model being used. In the case of a freely jointed chain, where the orientation of each segment is completely uncorrelated with the others, C_n equals 1. For more realistic models like the freely rotating chain, which incorporates a fixed bond angle between adjacent segments, C_n becomes greater than 1 and increases with the degree of correlation between successive bonds, ultimately approaching a limiting value. (Rubinstein/Colby, 2003)

Another important measure of the spatial distribution of a polymer chain is the radius of gyration R_g. This quantity represents the average squared distance of each monomer from the chain's center of mass, providing a sense of how the monomers are spread out in space. For an ideal chain modelled as a random walk of Kuhn segments, the mean-squared radius of gyration is given by

$$\langle R_g^2 \rangle = \frac{Nb^2}{6},$$

where N is the number of Kuhn segments and b is the Kuhn length, an effective segment length that accounts for the stiffness and persistence of the polymer

chain. The Kuhn length is generally larger than the actual bond length, as it represents the length over which the chain behaves as if it were freely jointed. In this idealized framework, the relationship between the end-to-end distance and the Kuhn segment description simplifies to

$$\langle R^2 \rangle = Nb^2,$$

which directly connects the overall size of the chain to the number and length of its effective segments. Combining this with the earlier expression for the radius of gyration leads to the well known relation

$$\langle R_g^2 \rangle = \frac{\langle R^2 \rangle}{6},$$

which is characteristic of Gaussian or ideal chain statistics. This proportionality is widely used in both theoretical models and experimental interpretations to relate different size metrics of polymer chains.

Furthermore, the probability distribution P of the end-to-end vector $\vec{R}$ for an ideal polymer chain is accurately described by a Gaussian function. For $|\vec{R}| \ll R_{max} = Nb$ the distribution is

$$P(N, \vec{R}) = \left(\frac{3}{2\pi N b^2} \right)^{3/2} \exp\left(-\frac{3\vec{R}^2}{2Nb^2} \right),$$

which highlights the random walk nature of ideal chain configurations.

1.2.2 Real Polymers

Polymer chains are macromolecules composed of repeated monomer units, and their behavior in solution is largely determined by the interactions between monomers and the surrounding solvent. These interactions, which can be both attractive and repulsive, play a crucial role in defining the polymer's conformation and its physical properties. One key concept in understanding polymer behavior is the excluded volume v, which represents the effective space around each monomer that other monomers cannot occupy. The excluded volume is temperature-dependent and, near the θ-temperature θ, is given by

$$v \approx b^3 \left(\frac{T - \theta}{T} \right),$$

where b is the segment length, and T is the temperature. At the θ-temperature, the attractive and repulsive forces between monomers cancel each other out, making the excluded volume effectively zero. This special condition is known as the θ-state, where the polymer chain behaves like an ideal random walk with no net interaction. In this case, the coil size or end-to-end distance scales as

$$R_0 = bN^{1/2},$$

where N is the number of monomers in the chain.

When the temperature rises above θ, repulsive interactions between monomers dominate, leading to a positive excluded volume. As a result, the chain expands and behaves as a self-avoiding walk (SAW), corresponding to a good solvent, where the polymer is well-solvated. The scaling of the coil size or end-to-end distance in this regime is

$$R_F \approx b \left(\frac{v}{b^3}\right)^{\frac{2\nu-1}{6\nu-2}} N^{\nu},$$

with $\nu \approx 0.588$ is the Flory exponent in three dimensions. In the case of a good thermal solvent, this scaling can be approximated as

$$R_F \approx b \left(\frac{v}{b^3}\right)^{0.19} N^{0.588}.$$

In such a good solvent, the chain can be thought of as a sequence of thermal blobs, locally ideal segments whose size decreases as the temperature increases due to enhanced repulsion. In an athermal solvent, the solvent quality does not change with temperature, and the excluded volume remains constant. The polymer chain still adopts a swollen SAW conformation, and its size scales similarly as

$$R \approx bN^{0.588}.$$

Conversely, when the temperature falls below θ, attractive forces between monomers outweigh the repulsive interactions, leading to a negative excluded volume. This causes the polymer chain to collapse into a compact globular structure, which is typical of a poor solvent. The size of the polymer coil in this regime scales as

$$R_g \approx |v|^{-1/5} b^2 N^{1/3}.$$

In the extreme case of a non-solvent, where the polymer is fully collapsed, the chain behaves like a dense sphere, and its size scales as:

$$R \approx bN^{1/3}.$$

These transitions between expanded, ideal, and collapsed conformations illustrate the sensitivity of polymer behavior to solvent quality and temperature. Understanding this interplay is essential for controlling polymer properties in various applications.

Chains and Excluded Volume Effects: Real polymer chains differ significantly from ideal models due to the presence of intra-chain interactions. A key interaction is the excluded volume effect, which prevents monomers from occupying the same spatial location. As a result, the polymer avoids itself and adopts a more extended conformation compared to an ideal chain. In this regime, the polymer adopts a self-avoiding walk conformation. The excluded volume leads to a non-Gaussian distribution for the end-to-end vector. While

the exact analytical form of $P(\vec{R})$ for SAWs is not known, it can be approximated by a stretched exponential function for large N

$$P(R) \sim R^{\theta} \exp\left(-A\left(\frac{R}{N^{\nu}}\right)^{\delta}\right),$$

where θ is a model-dependent exponent and $\delta = 1/(1-\nu) \approx 2.43$. The constant A encapsulates geometric and interaction-specific prefactors. This distribution reflects the asymmetry and long tail compared to the Gaussian case, indicating a higher probability for larger extensions due to the self-avoiding nature of the chain. The average end-to-end distance in this case scales as [7]

$$\langle R^2 \rangle \sim N^{2\nu} \approx N^{1.176}.$$

Radius of Gyration: A related measure of the polymer's size is the radius of gyration, R_g, which is defined as the root-mean-square distance of the monomers from the center of mass of the chain. For real chains with excluded volume, R_g scales similarly to the end-to-end distance

$$\langle R_g^2 \rangle \sim N^{2\nu}.$$

The distribution of R_g also deviates from Gaussian behavior, reflecting the influence of solvent quality and temperature.

Quality and Chain Statistics: The probability distribution of polymer conformations is highly sensitive to the quality of the solvent, which affects the sign and magnitude of the excluded volume:

- **Good solvent** ($v > 0$): The chain swells due to dominant repulsive interactions. The end-to-end distribution is broad with a long tail.
- **Theta solvent** ($v = 0$): Attractive and repulsive forces balance out. The chain behaves ideally, and the distribution is Gaussian.
- **Poor solvent** ($v < 0$): Attractive forces dominate, leading to chain collapse. The end-to-end distribution becomes narrow and highly peaked.

1.2.3 Monte Carlo Simulation

Monte Carlo (MC) simulations are a class of computational algorithms that use random sampling to estimate the behavior of complex systems. In statistical physics, they are particularly useful for exploring systems with many degrees of freedom, where exact solutions are intractable. By generating random configurations and accepting them based on physically motivated rules, such as the Boltzmann probability distribution, MC methods allow researchers to estimate equilibrium properties without solving the system analytically.

In the context of polymer chains, MC simulations are especially well-suited because they can efficiently sample the vast space of possible conformations a polymer can adopt. Real polymer chains, unlike ideal ones, exhibit excluded volume effects and solvent-dependent interactions that make their conformational statistics highly non-trivial. Rather than attempting to account for every possible chain configuration, which becomes infeasible for long chains, MC methods generate a statistically representative ensemble of conformations based on random moves and energy-based acceptance criteria. This process can be understood intuitively as a form of "smart guessing": the algorithm explores the conformational space of the polymer chain, but with a bias toward physically likely states. Over many iterations, the simulation converges to an equilibrium distribution, from which properties like the average end-to-end distance, radius of gyration, and full conformational distributions can be computed.

Monte Carlo simulations are particularly powerful for capturing how polymer chains behave under different solvent conditions. They can reproduce key phenomena such as the swelling of chains in good solvents, ideal behavior at the theta point, and collapse into compact globules in poor solvents. These transitions are governed by changes in excluded volume interactions, which MC methods can model effectively through appropriate potential functions and sampling strategies.

In summary, MC methods offer a flexible and efficient approach for studying polymer chains by enabling the exploration of complex conformational landscapes and capturing the statistical behavior of systems where analytical approaches are limited.

Statistical Quantities for Monte Carlo Simulations: Monte Carlo simulations are based on concepts from statistical mechanics. These averages reflect the system's behavior across all possible configurations, weighted by their physical likelihood. In this part some fundamental statistical quantities, that are used for this work, are presented:

The partition function Z is a central quantity in statistical mechanics, serving as a normalization factor for probabilities. It accounts for all possible states of the system, weighting them by their energy and temperature. The partition function is given by:

$$Z = \sum_i e^{-E_i/k_B T},$$

where E_i is the energy of the i-th state, k_B is Boltzmann's constant, and T is the temperature. Although the partition function is not directly computed in Monte Carlo simulations, it underlies the probabilistic sampling of polymer conformations. During a Monte Carlo simulation, configurations of the polymer chain are sampled with probabilities proportional to the Boltzmann factor e^{-E_i/k_BT}.

A key goal of Monte Carlo simulations is to compute thermal averages of various physical properties, such as the end-to-end distance, radius of gyration, or other observables. The thermal average $\langle A \rangle$ of an observable A is the expectation value over all possible configurations, weighted by their Boltzmann probability

$$\langle A \rangle = \frac{1}{Z} \sum_i A_i e^{-E_i/k_BT}$$

In Monte Carlo simulations, instead of summing over all configurations directly (which is impractical for large systems), these averages are estimated by sampling a subset of configurations. Over a large number of accepted configurations M, the average of A is approximated as

$$\langle A \rangle \approx \frac{1}{M} \sum_{j=1}^{M} A_j,$$

where A_j is the value of the observable in the j-th configuration.

The variance of an observable A reflects how much it fluctuates across different sampled configurations and is given by

$$Var(A) = \langle A^2 \rangle - \langle A \rangle^2$$

The variance provides insight into the uncertainty in the measured value of A. Monte Carlo simulations also rely on variance to estimate statistical error in the results. They allow for the calculation probability distributions of observables, such as the distribution of the end-to-end distance. [5]

1.2.4 Metropolis Criterion

In this thesis, the Metropolis criterion is used as the core acceptance rule within the Monte Carlo simulations applied to model polymer chains. As discussed earlier, real polymers exhibit complex behavior due to excluded volume effects and solvent interactions, which make analytical solutions difficult. The Metropolis criterion allows us to simulate these systems by generating statistically probable configurations according to the Boltzmann distribution.

Specifically, when a trial move changes the configuration of the polymer, for example, by repositioning a monomer, the change in energy ΔE is calculated. If $\Delta E \leq 0$, the move is accepted unconditionally, as it leads to a lower energy state. If $\Delta E > 0$, the move is accepted with probability

$$P_{accept} = e^{-\Delta E/k_BT}, \tag{1}$$

ensuring that energetically unfavourable moves can still occur, allowing the system to explore its full conformational space. This method reflects the statistical mechanics principles previously discussed and is essential for studying thermal averages and distributions of observables like the end-to-end distance and radius of gyration under various solvent conditions.(Frenkel/Smit, 2002)

1.2.5 WCA and FENE Potentials

To accurately simulate the behavior of real polymer chains in three dimensions, this thesis incorporates both excluded volume effects and finite bond flexibility. These are essential physical features introduced in the theoretical background, where it has been discussed how real polymers deviate from ideal chain models due to the finite size of monomers and the constrained but flexible nature of bonds. Capturing these effects is crucial for generating realistic polymer conformations, particularly in regimes where self-avoidance and bond extensibility play a significant role. In this context, the simulations in this thesis use a combination of two well-established interaction potentials: the Weeks-Chandler-Andersen (WCA) potential and the Finite Extensible Nonlinear Elastic (FENE) potential. These methods are used throughout the thesis to generate and analyse polymer configurations via the Metropolis Monte Carlo method.

The WCA potential is used to model the repulsive interaction between non-bonded monomers. This interaction enforces the excluded volume effect by preventing monomers from occupying the same spatial region. The WCA potential is derived from the Lennard-Jones potential but truncated and shifted to include only the repulsive part, resulting in a purely repulsive interaction. It is defined as

$$U_{WCA}(r) = \begin{cases} 4\epsilon \left[\left(\frac{\sigma}{r}\right)^{12} - \left(\frac{\sigma}{r}\right)^{6} \right] + \epsilon, & \text{for } r \leq 2^{1/6}\sigma \\ 0, & \text{for } r > 2^{1/6}\sigma, \end{cases} \tag{2}$$

where r is the distance between two monomers, σ is the effective diameter of a monomer, and ϵ determines the strength of the repulsive interaction. The potential smoothly approaches zero at the cutoff distance $r = 2^{1/6}\sigma$, ensuring a continuous energy landscape without introducing any attractive forces. This reflects the behavior of polymers in good solvents, where monomers repel each other due to steric hindrance and excluded volume effects.

To model the interaction between bonded monomers, the FENE potential is used. This potential captures the elasticity of bonds while preventing them from stretching beyond a finite limit. The FENE potential is given by

$$U_{\text{FENE}}(r) = -\frac{1}{2} k R_0^2 \ln \left[1 - \left(\frac{r}{R_0} \right)^2 \right], \quad \text{for } r < R_0, \tag{3}$$

where r is the distance between bonded monomers, k is the spring constant that controls bond stiffness, and R_0 is the maximum extension allowed for the bond. As the bond length approaches R_0, the potential diverges, effectively restricting

bond extension to a physical limit. This provides a nonlinear elastic behavior typical of real polymer chains, where bonds can fluctuate due to thermal motion but cannot extend indefinitely.

The combination of WCA and FENE potentials results in a coarse-grained polymer model that maintains chain connectivity while realistically accounting for both excluded volume and bond extensibility. This framework allows to move beyond ideal models and simulate physically realistic chain conformations. It serves as the basis for all simulations in this thesis, enabling analysis of conformational properties.

2 Single- and Double-Ring Polymers

2.1 Simulation Code

This work started with simple random walks of monomers and continued with simulations of linear polymer chains. The goal of these first steps was to build a better understanding of how polymer systems behave, especially before moving on to more complex structures like single and double rings. After learning from these simpler systems, the project continues with simulating two-ring systems using Monte Carlo and Metropolis algorithm. In the following, a pseudocode of the final simulation is shown:

Input: Simulation parameters (number of monomers, number of steps, ...)
Initialize: Topological properties
for each Monte Carlo step from 0 to $numberofsteps$ **do**
  Randomly select a monomer i
  Save current energy E_{old}
  Propose random displacement for monomer i
  Apply periodic boundary conditions
  Calculate new energy E_{new}
  $\Delta E = E_{\text{new}} - E_{\text{old}}$
  if $\Delta E < 0$ **or** $rand() < \exp(-\Delta E/(k_B T))$ **then**
    Accept new configuration
  else
    Reject move
  end if
  Store current energy value
  Compute centers of masses of each ring
  Compute gyration tensor for each ring
  Store eigenvalues and squared radii of gyration
end for
Save data to text files:
  Angles between centers of mass
  Squared gyration radii
  Gyration tensor eigenvalues
Plot energy change
Visualisation of polymers

The parameters used in this simulation (Table 1), which define the physical and statistical properties of the system, are, as follows:

Parameter	**Symbol**	**Value**
Number of monomers (per ring)	N	17
Number of Monte Carlo steps	n	10^5
WCA – Effective diameter of monomer	σ	1
WCA – Strength of repulsive interaction	ϵ	1
WCA – Cutoff distance	r	$2^{1/6}\sigma$
FENE – Spring constant	k	40
FENE – Maximum extension length	R_0	2.5σ
Temperature	T	1
Boltzmann constant	k_B	1

Table 1: Simulation parameters used in the Monte Carlo simulations

In this simulation, the energy between monomers is calculated using the WCA potential, while bonded pairs of monomers also include the FENE potential. The Monte Carlo method works by randomly selecting a monomer and trying a small random movement. If the movement lowers the energy, it's accepted. If it increases the energy, it's accepted with a probability depending on the energy difference, following the Metropolis algorithm. More detailed information about this can be found in the Introduction.

The main quantities calculated in this simulation are the angles between the centres of mass of the two rings for the double-ring polymer, and for all polymer topologies, the gyration tensor, its eigenvalues, and the squared radius of gyration derived from them. These values are saved every 100 Monte Carlo steps. Based on the raw data, properties such as the bending rigidity of the double-ring structure, for every polymer configuration shape descriptors like prolateness and anisotropy, can be computed later.

2.2 Analyses of Polymer Systems

A polymer is made of many connected segments. The angle between neighbouring segments, in this case two rings that are connected over a bonded pair, fluctuates due to potential motion. A stiff polymer prefers small angle changes and in contrary a flexible one allows larger bending. To measure the bending, this work defines center of masses for each ring and analyses the distribution $P(\alpha)$ of the angles between these center of masses.

The radius of gyration, which corresponds to end-to-end distance, measures how far the polymer's monomers are spread out from their center of mass. For this system this property can be calculated with [1]

$$R_g^2 = \frac{1}{N} \sum_{i=1}^{N} \left| \mathbf{r}_i - \mathbf{r}_{\mathrm{COM}} \right|^2 . \tag{4}$$

Here N being number of Monomers, $\mathbf{r}_i$ the position of monomer i and $\mathbf{r}_{\mathrm{COM}}$ center of mass.

2.2.1 Gyration Tensor

A very useful tool to analyse the polymer structure is the gyration tensor G. It describes the second moments of position of monomers [1]:

$$G_{mn} = \frac{1}{N} \sum_{i=1}^{N} \mathbf{r}_m^{(i)} \mathbf{r}_n^{(i)} \tag{5}$$

G is a symmetric 3x3 matrix, and as such, it can be diagonalised and expressed as

$$\mathbf{G} = \begin{bmatrix} \lambda_x & 0 & 0 \\ 0 & \lambda_y & 0 \\ 0 & 0 & \lambda_z \end{bmatrix},$$

with λ_i being the eigenvalues of the tensor. For further investigation, the eigenvalues are ordered by their size, so that the same axes are chosen equivalently for every system. In this terminology, the largest eigenvalue can be defined as λ_x and the smallest as λ_z. With this form, the radius of gyration R_g can ultimately be extracted from the trace of the gyration tensor [1]

$$R_g^2 = (\lambda_x + \lambda_y + \lambda_z). \tag{6}$$

2.2.2 Simulation Relaxation and Equilibration Approach

The initial positions of the monomers are chosen so that the system is optimally stimulated. To find the optimal distance between monomers, the total potential energy, given by the combination of FENE and WCA potentials, covering both attraction and repulsion, is calculated. By numerically minimizing this total potential energy, the distance (optimal bond length) that minimizes the potential

for the initial set-up can be found. This approach not only ensures a physically realistic starting point, but also facilitates monitoring of the system's energy evolution over time, allowing for the identification of an appropriate equilibration period suitable for statistical analysis. Figure 1 shows the initial positions of the monomers, which has been visualized with simulation code above.

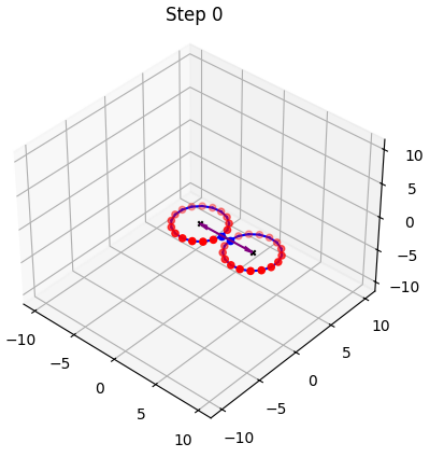

Figure 1: Initial positions of the monomers with an optimal bond length of 0.9651 in dimensions of k_BT . Each ring has 17 monomers. The visualized vectors originate from the midpoint of the bond connecting the rings and point toward the centres of masses of both rings. These vectors were later used for rigidity analysis of the whole structure.

However, in the simulated polymer systems, the relaxation process required a significant amount of time, as indicated by the correlation time function, which is defined as

$$C(\tau) = \frac{\langle (x_t - \mu)(x_{t+\tau} - \mu) \rangle}{\langle (x_t - \mu)^2 \rangle}, \quad with \quad \mu = \langle x_t \rangle.$$

Here $\langle \cdot \rangle$ is the mean of time t, τ the time delay and x_t the position of monomer at time t. C(0) is 1 by construction and means absolute correlation of the system. C(t) being 0 displays that the system is fully decorrelated and with that fully relaxed.

Since it was not feasible to wait for complete decorrelation of the system, the focus was placed on reaching thermal equilibrium. To determine when the system reached equilibrium, the total potential energy was monitored throughout the simulations. Once the potential energy stopped decreasing and began oscillating around a relatively stable value, the system was considered to be in

equilibrium. Although this point may not reflect full relaxation in terms of long-time correlation decay, it was assumed sufficient for reliable property analysis.

From that point onward, all properties were analysed based on the equilibrated segment of the trajectory. This approach was chosen to balance accuracy with computational practicality, and is commonly used in polymer simulations where complete decorrelation times can be prohibitively long.

2.2.3 Anisotropy

Another parameter that describes the topology of the polymer is the anisotropy b, which is just a degree of shape asymmetry and defined by [1]

$$b = 1 - \frac{3(\lambda_x\lambda_y + \lambda_y\lambda_z + \lambda_z\lambda_x)}{R_g^4}. \tag{7}$$

b being 0 would mean that the system is perfectly spherical, and b being 1 that the system is highly elongated or flat. Thus, anisotropy can indicate elongation or flattening, which will provide more information about the topological change of the polymer.

2.2.4 Prolateness

To tell whether the polymer is stretched (prolate) or flattened (oblate) can be expressed with prolateness S, which is defined by [1]

$$S = \frac{(3\lambda_x - R_g^2)(3\lambda_y - R_g^2)(3\lambda_z - R_g^2)}{R_g^6} \tag{8}$$

S being larger than 0 would mean that the system is prolate (rugby-ball shaped), smaller than 0 that it is oblate (disk-like), and 0 that it is spherical.

2.2.5 Bending Rigidity

From statistical mechanics, the angle distribution follows the Boltzmann distribution:

$$P(\alpha) \propto e^{-\beta K \cos(\alpha)}, \quad with \quad \beta = \frac{1}{k_B T}. \tag{9}$$

Here, K is bending stiffness and $\cos(\alpha)$ is the alignment measure between neighboring segments, since bending energy scales with $\cos(\alpha)$, minimizing energy when the chain is straight.

From the data gathered with the simulation code, histograms of the angle distribution are computed. To determine the value of the bending rigidity K from equation 9, the natural logarithm of the normalized angular distribution $P(\alpha)$ is taken, resulting in the expression:

$$\log(P(\alpha)) = -\beta K \cos(\alpha) + const. \tag{10}$$

This equation suggests that a plot of $\log(P(\alpha))$ against $\cos(\alpha)$ produces a linear relationship, with the slope given by -βK. Applying a linear regression to the data in these transformed coordinates yields an estimate for K through the relation:

$$K = -\frac{\text{slope}}{\beta} \tag{11}$$

This method provides a straightforward and effective way of estimating the bending stiffness of the polymer using only statistical data on segmental angles. The resulting value of K serves as a quantitative measure of the chain's resistance to bending deformations, without requiring explicit knowledge of the energy function's absolute values.

2.2.6 Analysis Code

The data generated during the simulation, such as angles between centers of mass, squared radii of gyration, and gyration tensor eigenvalues, is analysed in a separate post-processing step. The goal of this analysis is to extract meaningful physical properties such as the bending rigidity of the double ring system, as well as structural descriptors like anisotropy and prolateness.

In the following, a pseudocode of the analysis process is provided:

Input: Angle files, R_g^2 data files, eigenvalue files
Initialize: Physical constants $\beta = 1/(k_B T) = 1$
for each "angle" file **do**
  Load angles
  Compute histogram of angles and corresponding $\cos(\alpha)$
  Compute $\log P(\alpha)$ from histogram
  Perform linear fit: $\log P(\alpha) = -\beta K \cos(\alpha) + C$
  Store slope and compute bending rigidity $K = -\text{slope}/\beta$
end for
Compute mean and standard deviation of all K values
Save results
for each gyration radius file **do**
  Load R_g^2 values
  Plot and save histograms for R_g^2 of each component
end for
Define helper functions:
  Sort eigenvalues in descending order
  Compute anisotropy b from sorted eigenvalues
  Compute prolateness S from sorted eigenvalues
for each eigenvalue file **do**
  Load eigenvalue data
  Sort eigenvalues $\lambda_1 \geq \lambda_2 \geq \lambda_3$
  Compute mean sorted eigenvalues for each structure
  Compute anisotropy b and prolateness S for each step
  Save results
end for

This code allows us to extract structural information from the raw simulation data. The bending rigidity K is estimated from the angular distribution using a Boltzmann-weighted fit of the probability density function. The shape properties of the polymer system are quantified using the radius of gyration, anisotropy and prolateness, all derived from the gyration tensor's eigenvalues. The R_g^2 histograms provide insight into the overall size fluctuations of the system.

All output data and figures from this analysis are stored for further inspection, which will be provided in the section Results.

2.3 Results

Before presenting the results mentioned in the previous sections, and to bring more frankness into the work, the correlation time, which shows how decorrelated the statistical properties of the structure are, should be shown for an example simulation. Figure 2 shows how the system decorrelates with each Monte Carlo step.

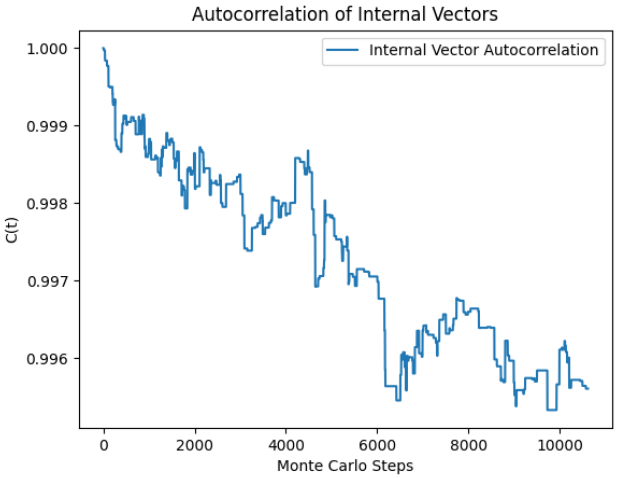

Figure 2: Autocorrelation C vs. 10^4 MC-Steps: Initially the function is 1 and decreases with the movement of the polymer. It is seeable, how slow the downscaling is.

As explained earlier and can be seen, it wasn't feasible to wait for perfect decorrelation, since that would require a much faster code or simply a lot more time.

The equilibrium of the system can be seen from the fluctuations in potential energy. The period of continuous oscillation in the potential energy is taken into account for further investigation. Figure 3 is an example polymer showing the energy change over time.

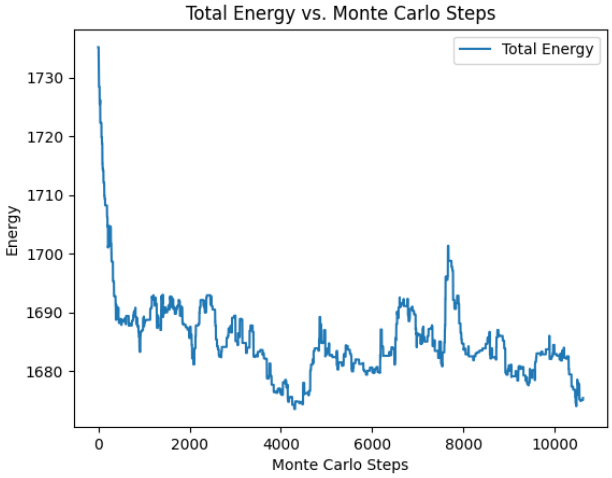

Figure 3: Energy in dimensions of $k_B T$ vs. 10^4 MC-Steps: The begin of the continuous oscillation refers to thermal equilibrium, which allows this work to make physical statements.

The structure of the polymer after 10^4 MC-Steps, to which the visualisations above belong, can be seen in Figure 4.

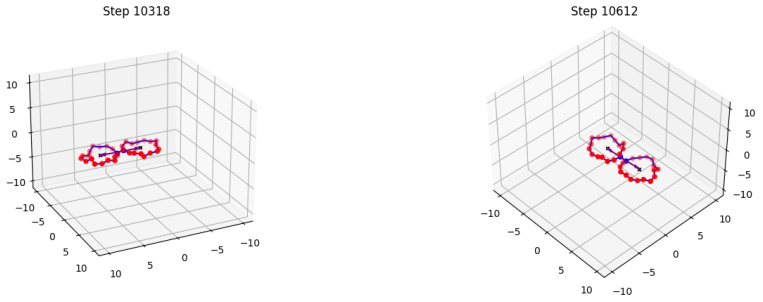

Figure 4: Double ring polymer visualized from different point of views after 10^4 MC-Steps.

These illustrations serve as examples, indicating that this particular polymer has not undergone further inspection. Detailed analyses have been conducted on seven other double ring polymers and seven single ring polymers.

2.3.1 Double Ring

Bending Rigidity: Before presenting the results on bending rigidity K, the existence of K should be discussed. Regardless of the details, by assuming system has an energy that depends on angles between segments, and by expanding the Hamiltonian in a Taylor-Series in those angles, the lowest non-trivial term will be quadratic and its coefficient is the bending stiffness K. So it must exist if the system penalizes bending at all. With this assumption, the simulation has been conducted and seven datasets collected. Two of these datasets show that there are two angles that the polymer is distinctly striving towards. These datasets can be seen in Figure 5.

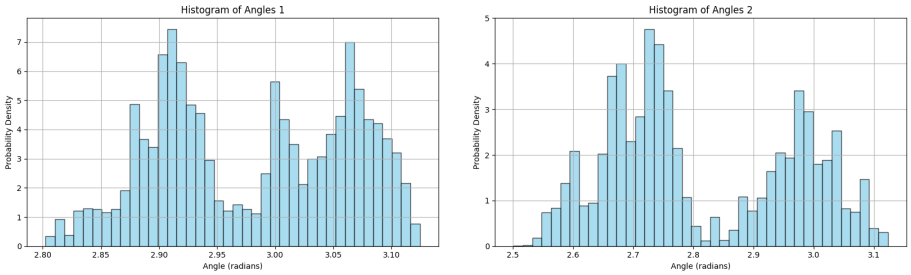

Figure 5: Two histograms representing the angular distributions of the center of mass of a double ring polymer, obtained from two separate datasets. The plots capture the oscillatory behaviour between two preferred angular positions, indicating a bistable or switching dynamic in the conformational motion of the polymer.

The rest of the datasets show oscillation around only one angle. Since the histograms exhibit similar profiles, one representative example is shown in 6, displaying one single dominant angular peak.

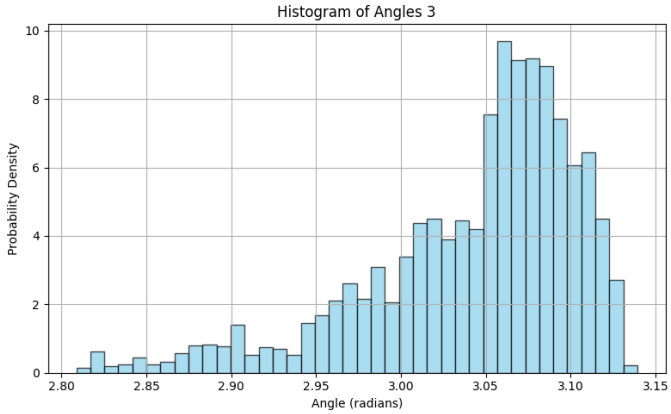

Figure 6: Histogram of a dataset showing one dominant angle that the double ring polymer tends to settle into. This indicates that, unlike in the oscillating case, the polymer mostly stays around a single angular configuration.

Calculating K for the datasets that show one dominant angle by equation 11 results in

$$K = 68.35 \pm 41.07.$$

Since the approach in this work is purely statistical and the data is not fully decorrelated, a large uncertainty in the value of K is to be expected. Nevertheless, the main goal, to show that the double ring polymer has a measurable bending rigidity, is fulfilled. The presence of a dominant angle and the resulting estimate for K support this conclusion.

Topological Analyses: To quantitatively characterize the structures, the eigenvalues of the gyration tensor are computed for each ring and the entire system, and for each dataset that exhibited a single dominant angle orientation. To identify general trends, the eigenvalues are sorted in descending order and averaged across the datasets. The resulting mean values provide insight into the average shape and orientation of the analysed polymer structures. These values are presented in Table 2.

System	λ_1	λ_2	λ_3
Ring 1	2.5607	1.7621	0.1425
Ring 2	2.6743	1.6949	0.1221
Total	11.2888	2.0010	0.1667

Table 2: Averaged sorted eigenvalues of the gyration tensor for each ring and the total system. The eigenvalues $\lambda_1 \geq \lambda_2 \geq \lambda_3$ characterize the principal axes of the polymer's spatial extension.

Both Ring 1 and Ring 2 have eigenvalues $\lambda_1 > \lambda_2 \gg \lambda_3$, which means they are not spherical but rather stretched out in one main direction. Ring 2 is slightly more extended along that main axis than Ring 1, but overall, their shapes are very similar. Looking at the total system, λ_1 tells us the full system is a lot more elongated along its first principal axis. Since the total eigenvalues are not just a simple sum of the two rings, it suggests that the rings are not acting independently, they are more likely aligned or interacting in a way that increases the overall extension.

The corresponding radii of gyration are displayed as histograms in Figure 7.

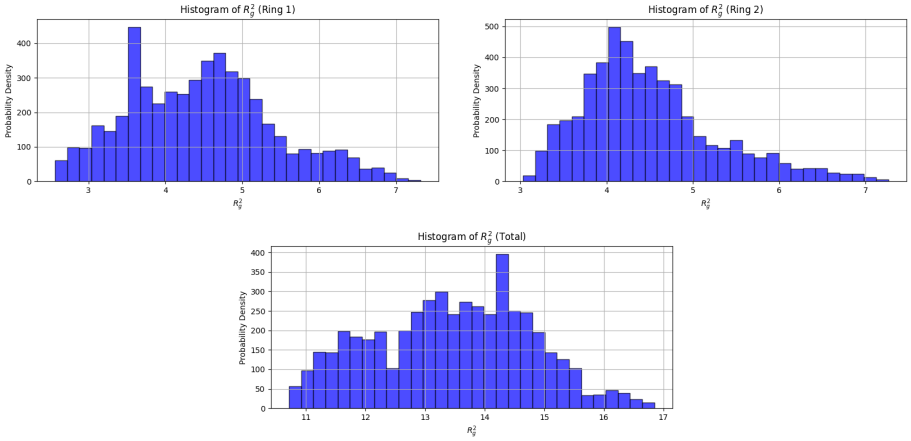

Figure 7: Histograms of the squared radius of gyration R_g^2 for each ring of double ring polymer and the total system, collected over all datasets that show one angle striving. The distribution reflects the variability in the spatial extension of the polymer configurations.

Ring 1 has a broader distribution than Ring 2, which means it explores a wider range of shapes and sizes. This suggests that Ring 1 is more flexible or less constrained in its motion. Ring 2, on the other hand, has a narrower and more peaked distribution, showing that its shape stays more consistent across different configurations. The total system shows a much wider distribution of R_g^2, with several local peaks. This means the full polymer can adopt many dif-

ferent overall shapes, from more compact to more extended.

R_g^2 values give a measure of how large and extended the entire polymer system is. Taking the mean of the histograms above, radii of gyration in k_BT dimensions result in:

$$R_g^2(Ring1) = 4.465 \quad , \quad R_g^2(Ring2) = 4.491 \quad , \quad R_g^2(Total) = 13.457$$

In addition, the averaged anisotropy parameter b and the prolateness S for the total system were calculated based on the properties described above. The values

$$b = 0.5891 \quad , \quad S = 0.8089$$

indicate also an anisotropic and prolate structure, meaning the polymer system is elongated rather than spherical.

Furthermore, as an illustrative example, the evolution of S and b over MC-Steps is shown for a selected dataset in Figure 8.

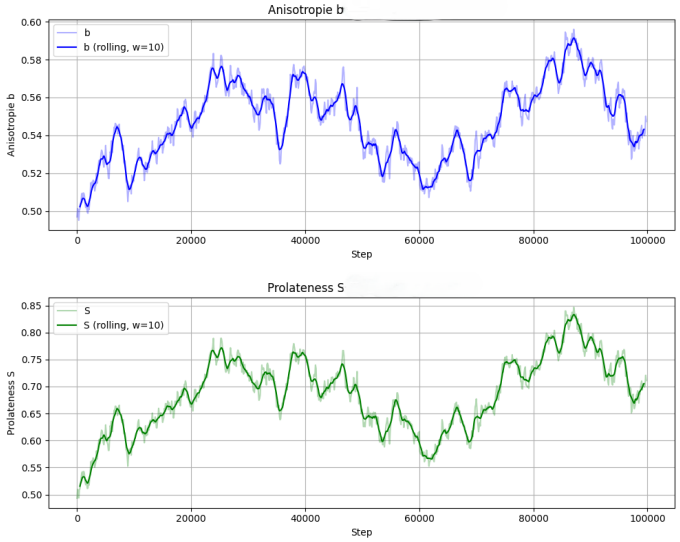

Figure 8: Evolution of the anisotropy parameter b and prolateness parameter S as a function of Monte Carlo steps for a selected dataset. Both raw data and smoothed data using a rolling average are shown. The plots illustrate the fluctuations and overall trends in shape descriptors during the simulation.

2.3.2 Single Ring

In the following, a similar analysis as presented for the double ring system is carried out, now focusing on the single ring polymer. Here the simulation datasets did not show any irregularities, thus all seven datasets have been undergone the procedure.

Again, to quantitatively describe the polymer shapes, the eigenvalues of the gyration tensor were computed, sorted in descending order and averaged across all datasets. Table 3 presents these values accordingly.

System	$\boldsymbol{\lambda_1}$	$\boldsymbol{\lambda_2}$	$\boldsymbol{\lambda_3}$
Ring 1	3.0983	2.3659	0.0797

Table 3: Averaged sorted eigenvalues of the gyration tensor for single ring polymer. The eigenvalues $\lambda_1 \geq \lambda_2 \geq \lambda_3$ characterize the principal axes of the polymer's spatial extension.

The sorted eigenvalues of the gyration tensor for the single ring polymer show a clear order, indicating an anisotropic structure, which suggests that the polymer is extended in two dimensions, with negligible thickness in the third. This configuration is characteristic of a planar and elongated shape.

In addition, distributions of the radius of gyration were evaluated. The corresponding results are shown in Figure 9.

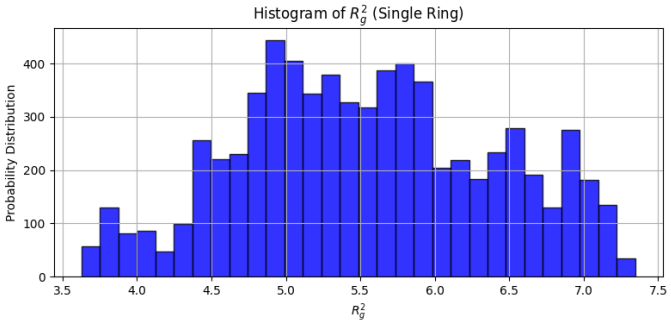

Figure 9: Histogram of the squared radius of gyration for the single ring polymer, collected over all simulations. The distribution reflects the variability in the polymer's spatial extension across different conformations sampled during the simulations.

The values of R_g^2 range roughly from 3.5 to 7.5, with most configurations centred around 5.0. This indicates that the polymer adopts both compact and more extended shapes. The distribution is fairly broad and shows several local

peaks, which could suggest that the polymer switches between different conformational states. Taking the mean results in (in k_BT dimensions):

$$R_g^2(Ring1) = 5.544.$$

The averaged anisotropy b and the prolateness S were also computed for the single ring system. These shape descriptors are useful for characterizing the deviation from spherical symmetry and are summarized as

$$b = 0.242 \quad , \quad S = -0.181.$$

The relatively low b value shows that the shape is not strongly elongated, and the negative S indicates a slightly oblate structure. This is consistent with the small third eigenvalue and supports the idea that the single ring mainly stays in a flat, planar configuration. Again, as an act of interest, the time evolution of anisotropy and prolateness of an illustrative data can be seen in Figure 10.

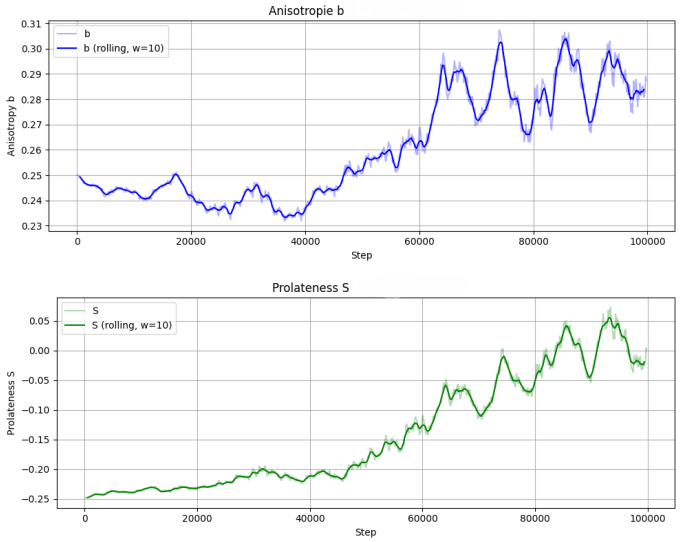

Figure 10: Evolution of the anisotropy parameter b and prolateness parameter S as a function of Monte Carlo steps for a selected dataset. Both raw data and smoothed data using a rolling average are shown. The plots illustrate the fluctuations and overall trends in shape descriptors during the simulation.

2.4 Conclusion

The present work aimed to investigate the structural and statistical properties of single and double ring polymers using Monte Carlo simulations. Through various datasets and statistical evaluations, a range of insights into polymer behavior was won, but some of these insights also challenge the models capabilities. Nevertheless, it was a total success to show, how effective statistical computational simulations are and can deliver great insight into systems that are not analytically solvable or complex studies.

A central result of the thesis is the bending rigidity K observed in the double ring polymer. While the theoretical model assumes a single angle term in the Hamiltonian describing bending stiffness, two of the collected datasets revealed behaviour that does not refer to this assumption. These datasets exhibited bistable angle distributions, suggesting that the system has two preferred angular configurations, indicating a more complex rigidity landscape than expected. Such behaviour hints at further terms or interactions influencing the polymer's angular dynamics.

For clarity, for both datasets showing two angle configuration, the angles have been plotted against MC-Steps. This can be seen in Figure 11. The remaining datasets consistently showed a clear single angular preference, from which a measurable bending rigidity $K = 68.35 \pm 41.07$ was extracted. Despite the large uncertainty, due to lacking decorrelation of the system, this result confirms that a characteristic stiffness in the double ring polymer does exist, supporting the idea that the polymer resists bending in a statistically significant way.

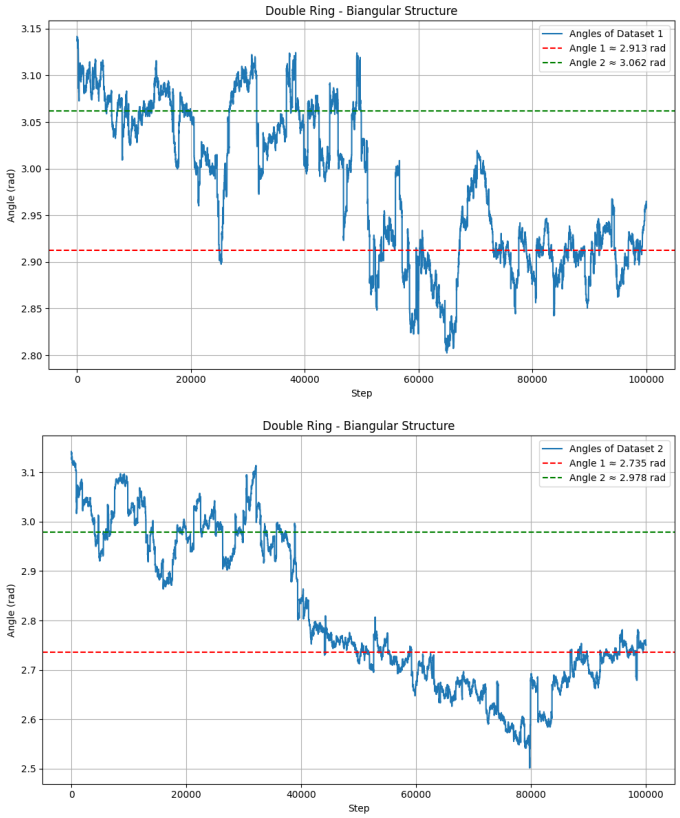

Figure 11: Angle evolution between centres of mass of the two rings for two double ring datasets. Both plots show how the system evolves between two distinct angular states over Monte Carlo steps, suggesting a bistable behaviour. These datasets support the assumption that the bending rigidity model with only one angular term might not be sufficient.

However, this work is based entirely on a statistical approach, meaning that the behaviour shown in the figure above does not necessarily represent a strict or deterministic rule, it could also be a result of statistical fluctuations or limited sampling.

The comparison between double and single ring systems reveals further important information. The eigenvalue analysis of the gyration tensor shows that both systems are anisotropic, but to different extents. In the double ring case, the total system has significantly larger variability than the individual rings. This supports the idea that monomer, or in other words inter-ring, interactions shape the global conformation of the polymer. The eigenvalues of the single ring polymer, on the other hand, show a very small third component λ_3, implying that the single ring is strongly planar. This planar behaviour could result from

entropic effects limiting the ring's ability to explore out-of-plane configurations.

Furthermore, comparing the squared radii of gyration R_g^2, it becomes clear that the single ring explores its configuration space more freely, likely due to the absence of inter-ring constraints that otherwise limit the degrees of freedom in the double ring system. While the double ring's total R_g^2 reaches higher values, its distribution is broader and more complex, highlighting the role of inter-ring topology in shaping the accessible conformational space.

Another significant observation is that the evolution of the shape parameters anisotropy b and prolateness S follow a very similar trajectory for both systems. However, the absolute values differ. The double ring displays stronger anisotropy and a clearly prolate structure, while the single ring is less anisotropic and slightly oblate.

It should also be noted that the numerical results presented here are based on relatively short Monte Carlo simulations, which did not fully decorrelate. As seen from the autocorrelation function, a significant amount of simulation time would be necessary to ensure proper statistical independence of configurations. A faster implementation, preferably in `C` rather than Python, would make it feasible to reach better decorrelation, allowing for more robust statistical conclusions. The current uncertainties reflect the limitations of the code.

To conclude, this study shows that even within simplified models, the double and single ring polymers behave distinctly. The interaction between rings in the double ring system results in more complex conformational dynamics and larger variability, while the single ring system maintains a more planar and consistent shape. These findings underscore the importance of topological constraints and inter-ring interactions in polymer physics and point to several directions for future refinement, including better-resolved statistical data, alternative modelling approaches for bending rigidity, and more efficient computational implementations.

3 Bibliography

References

[1] Christos N. Likos Andreas Zöttl Christoph Schneck, Jan Smrek. *Supercoiled ring polymers under shear flow*. Royal Society of Chemistry, 2024. Accessed January 10, 2025.

[2] Enzo Orlandini Cristian Micheletti, Davide Marenduzzo. Polymers with spatial or topological constraints: Theoretical and computational results. *Physics Reports*, 2011. Accessed March 7, 2025.

[3] Pierre-Gilles de Gennes. *Scaling Concepts in Polymer Physics*. Cornell University Press, 1979. Accessed January 10, 2025.

[4] Paul J. Flory. *Principles of Polymer Chemistry*. Cornell University Press, 1953. Accessed January 10, 2025.

[5] Daan Frenkel and Berend Smit. *Understanding Molecular Simulation*. Academic Press, 2002. Accessed January 10, 2025.

[6] Agnese Barbensi Dorothy Buck Julyan H.E. Cartwright Mateusz Chwastyk Marek Cieplak Ivan Coluzza Aleksandre Japaridze et al. Luca Tubiana, Gareth P. Alexander. Topology in soft and biological matter. *Physics Reports*, 2024. Accessed March 7, 2025.

[7] Michael Rubinstein and Ralph H. Colby. *Polymer Physics*. Oxford University Press, 2003. Accessed December 17, 2025.